The stresses developed round displacement piles penetrating in sand

Z.X. Yang[1], R.J. Jardine[2], B.T. Zhu[3], S. Rimoy[4]

Abstract

Establishing the stress conditions developed around displacement piles in sands is crucial to improving the understanding and modeling of their behavior. High quality experiments and theoretical analyses are giving new insights into the effects of penetration on stress conditions. This paper synthesizes findings from three independent experimental studies on normally consolidated silica sands and a trio of numerical analyses that tackle the problem from different perspectives. The significant degrees of uncertainty in the measurements and predictions are recognized and significant differences between data sets are discussed and largely resolved. Applying a consistent normalized interpretive framework leads to clear common trends regarding how installation affects the stress regime. While the main emphasis is placed on the radial effective stresses developed around pile shafts, the circumferential and vertical stress states are also considered.

Keywords: displacement pile; sands; stress analysis; stress path

1 Research Center of Coastal and Urban Geotechnical Engineering, Department of Civil Engineering, Zhejiang University, China, email: zxyang@zju.edu.cn

2 Department of Civil and Environmental Engineering, Imperial College, UK, email: r.jardine@imperial.ac.uk

3 NOMA Consulting Pty Ltd, Australia, email: Bitang.Zhu@noma-consulting.com

4 Department of Transportation and Geotechnical Engineering, University of Dar es Salaam, Tanzania; formerly Imperial College, UK, email: rimoy@udsm.ac.tz

Introduction

Field testing of piles equipped with high quality Surface Stress Transducers (SSTs) by Lehane et al (1993) and Chow (1997) revealed that extreme stress changes occur during penetration in sand, especially around the tips. The radial stress σ'_{rc} acting against the shafts at any given depth (z) after installation was shown to (i) vary directly with local CPT resistance, q_c, reflecting sand stiffness and state, and (ii) reduce systematically as the pile advanced and the relative height above the tip $h = z - z_{tip}$ increased. A weak dependence on the free-field vertical effective stress σ'_{zo} was also identified. Jardine et al. (2005) proposed Eq. (1) for use in design of cylindrical piles driven in silica sands:

$$\sigma'_{rc} = f(z) = 0.029 q_c (\sigma'_{zo}/p_A)^{0.13} (h/R)^{-0.38} \qquad \text{Eq (1)}$$

where p_A is the atmospheric pressure. The q_c and h/R terms have strong influences, while each tenfold change in σ'_{zo} leads to a change of just 35% in σ'_{rc}. It has been argued that the number of load cycles imposed during installation (White and Lehane 2004) and time effects (Jardine et al 2006) may also be influential, although these factors are generally neglected in practice. 'ICP' design rules incorporating Eq. (1), effective stress shaft failure criteria and new base capacity rules have been validated through comprehensive field test axial capacity database studies that demonstrated no systematic bias and gave a coefficient of variation < 0.30, far below the values applying to conventional approaches (Jardine et al 2005). This approach is now utilized in offshore engineering (Jardine et al 2005, Overy 2007, API 2011) where an equivalent radius R* is substituted into Eq (1) for coring open-ended piles, calculated from the pile's outer and inner radii (R_o and R_i) as $R^* = (R_o^2 - R_i^2)^{1/2}$. In the alternative 'UWA' approach a scalar reduction factor is applied to σ'_{rc} that depends on the pile geometry and Incremental Filling Ratio (IFR); Lehane et al (2005). The UWA and ICP approaches predict that the equivalent average end bearing resistances q_b of plugging tubular piles should decline in relation to q_c as pile diameter D increases, when all other factors are held constant. However, the alternative Fugro-05 (Kolk et al 2005) and NGI-05 (Clausen et al 2005) procedures do not anticipate any variation of q_b/q_c with D. In a similar way, the UWA, ICP and Fugro methods all indicate that local shaft resistance τ_{rzf} should fall (when all other factors are constant) as pile slenderness (L/D) increases, leading to a prediction that local shaft resistance should increase with D when L is held constant. This feature, which has been questioned by Knudsen et al (2012) is not incorporated into the NGI method. Further discussion on these and other related points is given by Jardine and Chow (2007).

Establishing the full stress field around the piles is crucial to settling the questions raised above and advancing understanding and modeling of driven pile soil-structure interaction, load-displacement response, group action and time dependent behavior. Accurate numerical analysis has the potential to provide powerful insights. But the extreme stresses, large strains, high degree of non-uniformity, moving boundaries, load cycling, interface shear, particle breakage and principal stress axis rotation involved all impose modeling difficulties. Most analyses have been limited to highly idealized cavity expansion treatments, which have been found to fit poorly with measurements made around pile shafts in careful experiments (Jardine et al 2013a, b). More plausible numerical investigations of pile penetration in sand are now feasible through advanced Discrete Element Method (DEM) and FEM techniques. DEM modeling allows particle and interface contact laws to be varied and can cope readily with large deformations and contact changes. Campos et al. (2005)'s DEM analyses examined the stress concentrations and particle movements around pile tips, while Kinloch and O'Sullivan (2007) investigated 'CPT' penetration mechanisms with 2-D analyses. Lau et al. (2010) emphasized the importance of rolling resistance in penetration simulations. Arroyo et al. (2011)'s 3-D DEM CPT modeling was able to show quantitative agreement with tip resistance experiments. Noting that DEM analyses of the surrounding stress field remains limited by the number of particles that can be considered, this paper focuses on assessing the degree to which advanced FEM analyses match the new experimental data. Three independent studies are considered:

- That by Sheng et al. (2005) who applied a Lagrangian multiplier pile-soil contact method to study steady penetration.
- The ‘zipper’ type technique employed by Henke and Grabe (2006, 2007), Henke (2008), Grabe and Henke (2010) and Qiu et al. (2011) in which a frictionless rigid ‘pilot’ tube of very small diameter was used to ‘guide’ the penetrating pile, while a Coulomb 'friction contact' was simulated between the pile and sand in combination with a Coupled Eulerian-Lagrangian (CEL) approach where the sand mass was discretized with an Eulerian mesh with appropriate element sizes, while both the pile and pile-soil interface were treated with Lagrangian descriptions.
- Zhang et al. (2013)’s Arbitrary Lagrangian Eulerian (ALE) FE approach. The latter applied re-meshing and variable remapping to simulate monotonic penetration, as well as a constitutive model incorporating breakage mechanics.

Table 1 gives further details of these studies. Zhang et al’s application of breakage mechanics followed experimental observations by Yang et al. (2010) that particle crushing, shear banding, and interface abrasion processes occurred beneath and around displacement piles in sands that could affect the pile-soil stress regime.

Experimental studies

Calibration Chamber experiments

This paper co*nsiders m*easurements made with normally consolidated silica sands in two sets of Calibration Chamber (CC) experiment and a single centrifuge study, as summarized in Table 1.

Experiments may be subject to unintended and possibly neglected influences from instrument calibration characteristics; chamber boundary conditions; pile tip geometry, material and roughness; and grain-scale effects. We discuss later the degree to which it is currently possible to measure the stresses consistently around displacement piles in sands.

CCs were introduced to calibrate penetration tests in uniform, well-characterized, sands under controlled pressure or displacement boundary conditions. CCs have been adapted for displacement pile studies by Golightly and Nauroy (1990), Foray et al (1993), (1998), Paik and Salgado (2003), Gavin and Lehane (2003), White and Bolton (2004), Paik et al (2011) and others. CCs offer better conditions than field tests to (i) measure stresses in the soil mass during installation (starting with Nauroy and Le Tirant 1983 and Foray 1991) and (ii) sample the sand after installation. However, analyses by Salgado et al (1998) and experiments by Rimoy (2013) show the importance of adopting either a large chamber-to-pile diameter ratio (ideally >100) or an active lateral boundary stress control system (Huang and Hsu 2005) to avoid potential deviations from field behavior. Joint research by Imperial College London and INPG Grenoble provides perhaps the most comprehensive CC study of the stresses developed around closed-ended displacement piles. Cone-ended 'Mini-ICP' stainless-steel, moderately rough ($R_{CLA} \approx 3\mu m$) piles with 36mm Outer Diameters (OD) were penetrated into dry pressurized, highly instrumented, medium-dense siliceous Fontainebleau NE34 fine sand. Cyclic jacking was employed and typically 50~200 strokes (with full unloading between each) were applied to penetrate ≈1m. Jardine et al (2009) reported the general experimental arrangements outlined in Fig. 1. The Mini-ICP instrumentation included reduced-scale SSTs to measure radial and shear shaft stresses at r/R = 1 and three levels on the pile shaft, h=6.7R, 21.7R and 41.7R respectively. Measurements were also made of σ'_z, σ'_θ and σ'_r at two to three levels in the sand mass at radial distances between 2 and 20R from the pile axis using miniature soil sensors. Zhu et al (2009) emphasize the highly non-linear and hysteretic behavior of stress measuring cells and note that complex calibration and data reduction procedures are required to obtain reliable data. Two membranes with different central Internal Diameters (IDs) were used to apply a surcharge pressure of σ'_{zo} ≈150 kPa to the sand mass. Separate CPT tests established q_c profiles for various boundary conditions. As shown in Fig. 2, both membrane designs gave quasi-constant CPT trace sections with q_c = 21±2 MPa, although this was achieved at a shallower depth with the smaller ID membrane. Also shown in the figure revised from Jardine et al (2013a) is the q_c profile predicted independently by Zhang et al (2013) that is examined comparatively later. Multiple load tests revealed axial capacities that compare encouragingly well with predictions made with the 'field-calibrated' ICP capacity approach. Jardine et al (2013a, b) report and interpret these experiments, which are referred to here as the 'Mini-ICP data-set' and provide the paper's main experimental bench-mark. Rimoy (2013) describes more elaborate experiments with the same equipment.

Gavin and Lehane (2003) report earlier, less extensive, CC stress measurements made around an open-ended relatively smooth (R_{CLA}≈0.4μm) stainless steel pile with an external diameter of 114 mm and wall thicknesses of 8.3 mm. The pile was jacked up to 1.6m into a 2.3 m high and 1.68 m diameter testing chamber filled with dry, uniform and fine to medium siliceous (d_{50}=0.22mm, C_u=1.6) sand placed at D_r=30±2%; sixteen jack strokes were employed. CPT q_c profiles were established independently. The open-ended pile showed 'coring' Incremental Filling Ratios (IFR) close to 100% down to z=0.6m and progressive plugging reduced the IFR to ≈14% at the final depth.

Centrifuge experiments

Centrifuges provide powerful insights into complex problems and help to identify fundamental underlying mechanisms. However, they also call into question potential particle-to-model scale effects, pile roughness issues, stress non-uniformities and side-wall constraining concerns that may affect any detailed measurements made. The q_c-depth profiles developed in field, calibration chamber and centrifuge tests also differ. Centrifuge CPT tests generally vary linearly with depth in uniform sands, see Fig. 3(a), while calibration chamber tests tend to give near parabolic q_c-σ'_{zo} relationships; Baldi et al (1986). Field data appear to resemble the CC trend more closely, as illustrated in Fig. 3 (b), which brings together for comparison a field CPT-q_c profile and an interpreted quadratic trend proposed by Doherty and Gavin (2010).

Centrifuge studies involving displacement piles in sand include those by Allard (1990), de Nicola and Randolph (1997), Klotz and Coop (2001), Sakr and Naggar (2003), White and Lehane (2004) and Levacher et al. (2008). Allard (1990) made soil stress measurements in experiments where she drove a smooth 9.5 mm diameter closed-ended stainless steel pile into a 152mm diameter centrifuge bucket filled with dry, uniform Nevada fine silica sand. The fine (d_{50} = 0.1mm) sand was placed at 1590kg/m^3 (with e_0 = 0.65, D_r = 57.5%). Vertical and radial stresses measured with strain-gauged diaphragm cells (2.6 to 5.1mm in diameter) whose strong cell action effects Allard identified and modeled in high acceleration centrifuge calibration tests. However, the pile driving soil stress maxima rose to almost double the calibration limits, leading to some measurement uncertainty.

Normalization of stresses

The experimental and theoretical studies summarized in Table 1 involve a range of pile details (closed and open, rough and smooth), initial effective stress levels (which vary by a factor of > 50 between cases), boundary conditions and sands with loose-to-dense states. Careful normalization is vital to synthesizing the data and identifying common trends. The experiments all show that the stresses around and below the piles vary sharply with (i) radial distance, *r*, from the pile axis, as well as (ii) relative height above (positive *h*) or below (negative *h*) the pile tip. Combining these observations with the field trends encapsulated in Eq. (1) suggests that σ'_z, σ'_θ and σ'_r can be normalized for variations in local q_c and free-field vertical stress σ'_{zo}, and represented by two dimensional functions with the form:

$$(\sigma'/q_c)/[\sigma'_{zo}/p_A]^{0.13}=f(h/R,r/R) \qquad \text{Eq. (2)}$$

By implication the equivalent radius R* should be substituted for R when dealing with predominantly coring open-ended piles. In principle, cyclic and monotonic installation procedures could produce different functions; time and scale effects could also be significant.This normalization is applied in the interpretation and comparisons given below. Most emphasis is placed on the radial effective stresses, but the circumferential and vertical stress states are also considered.

Comparison of experimental studies

Bench mark Mini-ICP set

We consider first the ‘bench-mark’ Mini-ICP data set. Pile penetration invoked extreme stress changes in all three normal stress components and significant stress changes out to r/R>30. Synthesis of thousands of ‘Mini-ICP’ installation stress measurements led to contour plots for all cylindrical stress components including the radial stress set given in Fig. 4 (reproduced from Jardine et al 2013b) where the results have been normalized for q_c. No correction is made for $[\sigma'_{zo}/p_A]^{0.13}$ in this plot. However, we note that the ratio remained close to unity (1.05 to 1.06) in these experiments. Plot (a) shows at two scales how the normalized stresses varied with r/R and h/R during ‘moving’ steady penetration stages while (b) represents the equivalent ‘stationary’ pause data recorded when the pile was unloaded fully;

the maximum stress loci are shown as dashed-line traces. The 'moving' σ'_{rm}/q_c and 'stationary' σ'_{rs}/q_c contours indicate intense stress concentrations emanating from the pile tip. The radial stress maximum recorded in the soil mass (at h/R~0.5, r/R=2) exceeded 16% q_c during penetration, while the 'zero-load' stationary values were 2 to 3 times smaller. A fully active failure zone develops beneath the advancing tip where, on average, $\sigma'_{zm}/q_c = 1$ and $\sigma'_{rm}= \sigma'_{\theta m} = K_A\sigma'_{zm}$ and $K_A = \tan^2(45 +\varphi'/2) \approx 1/3$ for Fontainebleau NE34 sand at critical state under high pressures; see Yang et al (2010) and Altuhafi and Jardine (2011).

Further comparisons between the 'moving' and stationary' stresses are presented in new plots given in Fig. 5 from sensors deployed in two tests at r/R ratios of 2 and 3 and depths (z) of 550 and 700mm. Close analysis shows that the stationary and moving radial stress measurements differ most significantly near the tip ($-5<h/R < 3$) where significant differences extend out to r/R = 10. Variation is mainly restricted to the r/R <2 region at higher levels on the shaft.The most reliable observations of how stresses vary with r/R at set h/R values were developed from the end of installation measurements. The stationary σ'_r and σ'_θ profiles interpreted by Jardine et al (2013b) for four h/R values are reproduced in Fig. 6(a) and (b). A key point to note is that the final radial stresses show maxima developing away from the shaft, between $2<r/R< 4$ and that σ'_θ must vary steeply with r/R to maintain equilibrium giving $\sigma'_\theta>\sigma'_r$ close to the shaft. This feature is critical to understanding the marked field ageing trends of driven piles. Chow et al. (1998) and Jardine et al (2006) proposed three possible mechanisms for the increases they observed in shaft capacity over time with piles driven in sand. One hypothesis was that shaft radial stresses increase during ageing as raised circumferential stresses relax through creep. The latter were thought to act in a sand arch formed around the displacement pile during installation, with the initially elevated hoop stresses shielding the pile shaft from higher radial stresses acting further away from the shaft. A similar mechanism was suggested independently by Åstedt et al. (1992) and was investigated in simplified cavity expansion/contraction analyses by White et al (2005). The data presented in Fig. 6 present the first experimental confirmation of the supposed stress regime.

CC experiments with an open ended pile

Gavin and Lehane set radial stress sensors at r/R = 7.6 at two depths (z/R=9.6 and 19.3) around their open-ended pile. Their measurements may be compared with the Mini-ICP trends after normalization, as described above, for their markedly different q_c and σ'_{zo} profiles. New comparisons are presented in Figures 7(a), (b), (c) and (d) to show how $(\sigma'_{rm}/q_c)/[\sigma'_{zo}/p_A]^{0.13}$ varied at equivalent sand mass positions as penetration progressed. The first pair of traces considers the deeper sensor location. Noting that the open pile was tending towards plugging (with an Incremental Filling Ratio of 38%) as it reached this depth, the open pile's outer radius is used to normalize the sensor's (h, r) coordinates in Fig. 7 (a); Fig. 7 (b) shows data from the equivalent (r/R = 8) Mini-ICP observation point. Data from the shallower of Gavin and Lehane's sensors are presented in Fig. 7 (c). The pile was fully coring at this depth (IFR = 100%) so the sensor's radial distance from the center-line is expressed as a multiple (14.6) of the equivalent solid pile radius R*. The closest matching Mini-ICP instrument (placed at r/R = 16) gave the results presented in Fig 7 (d).

Compared in this way, the two data sets show broadly similar responses. Both show marked differences between the moving and stationary stresses over the -5<h/R<5 range. They also show strong variations with h/R (or h/R*) which are slightly steeper with the Mini-ICP experiments. The Mini-ICP experiments developed higher normalized radial stress maxima than Gavin and Lehane's at the deeper location, with $(\sigma'_{rm}/q_c)/[\sigma'_{zo}/p_A]^{0.13}$ rising to 2.8% rather than 2.4% seen around the partially coring open pile. This difference may be related to the partially coring (IFR = 38%) open pile condition. However, both sets show $(\sigma'_{rm}/q_c)/[\sigma'_{zo}/p_A]^{0.13}$ maxima around 1% at the shallower location when radial coordinates are matched by equating r/R for the closed Mini-ICP and r/R* for the fully coring open pile. As noted earlier, Lehane et al (2005) preferred to account for open-ended pile conditions by effectively reducing the q_c term in Eq. (1) as the effective pile end area ratio falls, rather than adopting R*.

Overall, the degree of agreement is encouraging given the significant differences between the experimental arrangements. No upper surcharge or lubricated lateral boundaries were applied in Gavin and Lehane's tests. Their pile-to-chamber diameter ratio was lower and they adopted far looser sand and fewer jacking cycles. Their larger OD pile was also smoother and their stress cell calibrations less elaborate.

Centrifuge measurements

Allard (1990) presented traces against pile tip depth radial stress profiles from sensors installed at r/R = 2.67 and six z/R ratios. As she did not perform centrifuge CPT testing, we have projected a q_c profile from the centrifuge correlation by Gaudin et al. (2005), correcting for relative density by applying Baldi et al (1986). Fig.8(a) presents a re-working of Allard's stationary radial stresses, as recorded between blows applied under 50g acceleration and plotted here against h/R and normalized as $(\sigma'_{rs}/q_c)/[\sigma'_{zo}/p_A]^{0.13}$. Equivalent stationary Mini-ICP measurements made at comparable z/R and r/R locations are shown in Fig. 8 (b). The first point to recognize is the spread (among measurements made at equal r/R and h/R) of the measured stresses. The Mini-ICP tests show a spread about their mean values of around ±10% in their stress maxima; this spread increases to around ±50% as h/R increases towards 30. The Mini-ICP load cell calibrations also showed error bands increasing with the degree of unloading and pre-cycling (Zhu et al 2009). Although the centrifuge data show significantly more dispersed patterns, averaging of multiple measurements is essential with both data-sets. Despite the degree of scatter, the entirely independent experiments reveal common features, including similarly steep dependence on h/R. The centrifuge $(\sigma'_{rs}/q_c)/[\sigma'_{zo}/p_A]^{0.13}$ maxima developed at h/R ≈ 0 fall around 3.5% at r/R =2.67, while the equivalent Mini-ICP values average of around 8% at r/R = 2 to 3. Possible explanations for this significant discrepancy include:

(i) Errors in estimating the centrifuge q_c-σ'_{zo} profile
(ii) Limitations in the centrifuge stress-cell calibrations
(iii) Installation by driving rather than cyclic jacking
(iv) The different sands, piles, shaft roughnesses, initial stress fields, boundary conditions and scaling ratios.

Regarding the latter point, Allard’s centrifuge bucket/pile diameter ratio was relatively low at 16, while the Mini-ICP tests chamber-to-pile ratio 33. Her sensor diameter/d_{50} ratios were similar to the Mini-ICP range (38±12 compared with 30±1), but her pile diameter D had lower ratios than the Mini-ICP tests with respect to her (i) sand d_{50} (95 compared with 170) and (ii) soil sensor diameters (1.9-3.7 compared with 5.5-6). Bolton et al. (1999) argue that diameter/d_{50} ratios > 20 may be sufficient for centrifuge tests with smooth piles. Significant pile-sensor interference and dynamic driving densification effects might be expected in the centrifuge case, although no evidence is offered to support these speculations.

Comparisons with FEM analyses

The key trends from the above experiments may be compared with predictions from the three numerical analyses summarized in Table 1.

Lagrangian multiplier FEM analysis

Sheng et al. (2005) simulated the continuous in-flight penetration of a closed-ended pile of 0.03m diameter with a 60^o cone end into a centrifuge bucket filled with dry dense sand. Large-strain frictional contact was accommodated between the pile and soil with a reasonable interface friction angle of 27^o. However, mesh dimensions beneath the tip and near the pile shaft (with element widths set between R/4 and R/2) may have limited predictive accuracy. The sand was modeled as fully drained Modified Cam Clay (MCC), which Sheng et al considered could simulate the drained triaxial behavior of silica sand adequately, provided a pseudo-OCR is applied to ensure dilative behavior in the 'dry' side. However, all the experiments employed normally-consolidated sand masses. Sheng et al simulated a 0.56 m high and 0.58 m diameter centrifuge 'bucket' which had a chamber/pile diameter ratio of 19.3 (compared to 33.3 in the Mini-ICP tests). The sand was assumed to have e_0=0.75 (D_r = 76%). No surcharge was applied to the sand surface, but the initial stresses were scaled up to simulate centrifuge testing to 66.6g to approach prototype scale, giving σ'_{zo}=550kPa at the deepest point considered in Fig. 9(a).The Baldi et al (1986) expression was applied to estimate the q_c profile that would be expected from an idealized field CPT at prototype scale.

Examples of the stresses computed by Sheng et al. (2005) are plotted in new diagrams given in Fig. 9(a) as profiles with h/R of the 'moving' normalized radial stresses developed at r/R=1.13 for stages with tip depths z_{tip}=4, 8 and 16R: $(\sigma'_{rm}/q_c)/[\sigma'_{zo}/p_A]^{0.13}$ as the sand mass displacement pattern evolves from one involving shallow heave towards a deep penetration mechanism. Fig. 9(b) presents the Mini-ICP steady (deep) penetration 'moving' trends observed at r/R=2, which is the closest location where measurements could be made. The computed normalized maximum radial stress ratio (for deep penetration with z/R = 16) is 37.0% while that interpreted by Jardine et al. (2013b) for r/R=1.13 when h/R = 0.5 was slightly lower at 30.6%. The latter involved an interpolation between the closest measurement (of 17.8%) made at r/R = 2 and the $\sigma'_{rm} = K_A q_c$ maximum value applying on the conical pile tip face.

The numerical modeling and the Mini-ICP tests differ in several important respects: no surface surcharge was applied in the simulation, nor was any attempt made to match the cyclic jacking/driving process, or the interface shear phenomena of finite dilation, banding or particle crushing. The q_c profile is also uncertain. However, Sheng et al. (2005)'s analysis illustrates how the normalized stresses evolve with penetration. Their normalized deep penetration profile provides a good 'first principles' prediction of the observed steep variations with h/R that are due purely (under monotonic penetration) to the system geometry, as well as predicting stress maxima that agree reasonably with the experimental trend.

Coupled Eulerian Lagrangian (CEL) FEM analyses

Analyses employing a CEL technique of a 300 mm diameter closed conically-tipped pile penetrating monotonically in dry sand to 5m depth are reported by Henke et al. (2010) and Qiu et al. (2011). The soil was assumed to match uniform beds of Taiwanese Mai-Liao sand (Henke 2008) and a hypoplasticity constitutive law (Herle 1997) applied. Simulations were made for sand relative densities between 20 and 75% and Coulomb pile-sand interface friction was adopted assuming $\delta'=\varphi'/3$, although higher angles could be expected from practical interface shear tests (Ho et al 2011). CPT q_c profiles were estimated for our comparison from Baldi et al (1986).

The variations in the 'moving' sand radial stresses were reported separately by Henke et al (2010) and Qiu et al (2011) for radial profiles located at two depths extending out to 5m. Figs 10 (a) and (b) show the results for three relative densities reprocessed for this article as $(\sigma'_{rm}/q_c)/[\sigma'_{zo}/p_A]^{0.13}$ ratios plotted against r/R, considering horizontal profiles set at h/R = 6.67 and 13.33. Comparison with the Mini-ICP experiments is best made with the stationary profiles presented earlier in Fig. 6(a). It will be recalled that the stationary and moving radial stress measurements differ most significantly at h/R ratios between ± 3 and close to the shaft (r/R <2), so comparisons with the 'moving' numerical analysis profiles given in Figs 10 (a) and (b) are legitimate except, potentially, in the near-field r/R < 2 region.

As with Sheng et al (2005)'s analysis, significant differences exist between the numerical model and the Mini-ICP tests. These include: the 50~200 full load-unload cycles imposed in the Mini-ICP's installation; the perfectly uniform soils and un-surcharged sands simulated in the FE analysis as well as the interface shear and particle breakage processes. The soil model may not have been able to match fully the nonlinear, in-elastic and anisotropic behavior of real sands, including their dependency of the shear strength, stiffness, and dilatancy, stress state, void ratio and loading history. Despite these potential reservations, the numerical analyses capture a similar dependence of sand stress regime on the geometrical (h/R and r/R) and sand state (q_c and σ'_{zo}) variables. The reprocessed numerical results show (i) a clear decay in stresses with increasing h/R in the predictions for D_r = 40% (Fig. 10a), and (ii) comparable radial distributions to the experiments in Fig. 10 (b), including maxima developing away from the shaft at 2 < r/R < 4. Jardine et al. (2013b) show that the radial stress maxima seen in the 2 < r/R < 4 range in Figs. 5 and 10 necessarily imply steeply varying σ'_θ stress components with $\sigma'_\theta > \sigma'_r$ in the near field of pile shaft. The profile of radial stress with r/R (defined at h/R = 13.33) shows (for the most comparable D_r = 75% case) a maximum in $(\sigma'_{rm}/q_c)/[\sigma'_{zo}/p_A]^{0.13} \approx 2.5\%$ that exceeds the mid-point of the stationary experimental range (1.3 to 2% for h/R values between 5.6 and ≈20) by about 50%. Such quantitative discrepancies might be reduced in analyses that accounted for installation load-cycling or grain-crushing beneath the advancing tip (or in the shaft interface shear zone).

FE analysis incorporating grain crushing

Zhang et al (2013) adopted an Arbitrary Lagrangian Eulerian (ALE) FE approach with re-meshing and variable remapping to simulate monotonic penetration. Their breakage mechanics model provided good predictions for the evolving grain size distributions (GSD) trends and their tip resistance predictions matched the experiments well (see Fig. 2). One feature that was not captured analytically was the observed thickening of the interface shear band with increasing h/R that Yang et al (2010) related to interface abrasion and cyclic installation effects.

Discussion with Einav (2012) led to further processing of Zhang et al.'s simulations. Previously unpublished profiles of predictions for the 'moving' radial and circumferential effective stresses developed during the pile installation were communicated to the Authors and re-processed to give the normalized profiles of stresses varying with r/R at three h/R levels in Figs. 11 (a) and (b). These traces may be compared with the equivalent 'stationary' profiles interpreted from the Mini-ICP experiments given in Fig. 5. While the experimental and analytical profiles do not cover exactly the same h/R values (and should not be compared directly at r/R<2) they show many similarities. As with the analyses of Henke et al (2010) and Qiu et al (2011), radial stress maxima are predicted, although these develop slightly further away from the shaft (3 < r/R < 8). The computed σ'_θ profiles show the steep radial variations and $\sigma'_\theta > \sigma'_r$ trend interpreted by Jardine et al (2013b) close to the shaft. The radial stress profiles fall as h/R increases, as expected, although the variation at higher h/R values appears relatively gentle. The maximum value of $(\sigma'_{rm}/q_c)/[\sigma'_{zo}/p_A]^{0.13}$ predicted at h/R = 6 is 2.1%, which falls close to that observed experimentally (2%) at h/R = 5.6.

Further agreement between the predicted and measured near tip stress regimes is illustrated in three new normalized comparison plots in Fig. 12 that consider how the radial, circumferential and vertical effective stresses profiles vary with r/R at h/R values of 0 and 0.5.

Summary and conclusions

This paper has explored the cylindrical normal stresses developed around piles penetrating into normally consolidated silica sands, drawing together a trio of independent experimental investigations and three numerical analyses. The interpretation has synthesized measurements and predictions made at points with initial effective stresses ranging from 10 to 550 kPa and states from loose-to-dense by:

(i) Normalizing stresses with respect to local CPT q_c and non-dimensional vertical stress ratio $[\sigma'_{zo}/p_A]^{0.13}$.

(ii) Adopting the tip as the origin for non-dimensional spatial coordinates (h/R, r/R) for closed-ended conditions and (h/R*, r/R*) for open-ended piles.

The great care required to make reliable stress measurements has been emphasized. Experiments may be subject to a wide range of potential imperfections and sources of scatter or error. Equally, numerical modeling of the installation process poses a series of significant challenges. Despite these difficulties, quantification of the stress conditions developed around displacement piles in sand appears to becoming feasible. Clear trends are evident:

(1) 'Deep penetration' radial stress measurements and predictions, obtained by a wide range of approaches, show broadly similar strong dependence on relative pile tip depth, h/R, irrespective of the sand relative density and pile installation method (discontinuous jacking, driving or continuous pushing). Further studies are required to establish the detailed effects of the number of installation cycles and test boundary conditions.

(2) Use of the equivalent pile radius, R*, proposed by Jardine et al. (2005) allows the stresses developed around coring open piles to be reconciled with those developed with closed ends.

(3) The normalized radial stress maxima defined during steady penetration stages of both experiments and numerical analyses generally conform to within ± 50% of the equivalent measurements made at the same normalized locations in the 'bench mark' Mini-ICP experiments. Possible explanations have been suggested for any significant discrepancies identified between the disparate data-sets.

(4) Monotonic numerical analyses and cyclically advanced experiments both indicate that radial stress maxima develop away from the shaft in the $2<r/R<8$ range, leading to σ'_θ necessarily varying steeply with radius and $\sigma'_\theta>\sigma'_r$ conditions applying close to the shaft.

Scope exists for closer analysis by investigating further factors such as the performance of soil stress sensors, scale effects relating to the relative diameters of the piles with respect to the grain, test chamber and soil stress sensor diameters. Further studies to establish centrifuge CPT profiles and consider the effects of different installation styles would also be beneficial, as would further investigations of the potential effects of pile tip geometry and installation procedure, as well as prior overconsolidation of the sand mass. The incorporation of particle breakage into numerical simulations leads to interesting results. Further elaboration that allowed installation cycles, interface shear and sand anisotropy and other parameters to be considered more representatively appears warranted.

Acknowledgements

The research described was funded by Natural Science Foundation of China (No 51178421) and UK Royal Society, the Chinese Ministry of Education Distinguished Overseas Professorship Program, Shell U.K. Limited, the UK Health and Safety Executive, the UK Engineering Physical Sciences Research Council and Total, France. Their support is gratefully acknowledged as are the contributions made to the Mini-ICP experiments by colleagues at INPG Grenoble and Imperial College including: Professor Pierre Foray, Dr. Mark Emerson, Dr. Cristina Tsuha, Mr. Jean-Benoit Toni, Mr. Steve Ackerley, Mr Clive Dalton, Mr. Bernard Rey, Mr. Alan Bolsher, Mr. Matias Silva and Mr. Francesco La Malfa. Help from Professor Itai Einav in sharing his team's numerical analysis results is also acknowledged with thanks.

References:

Allard, M. A. (1990). *Soil stress field around driven piles*.PhD thesis, California Institute of Technology, California, USA.

Altuhafi, F., and Jardine, R.J. (2011). Effect of particle breakage and strain path reversal on the properties of sands located near to driven piles. Deformation Characteristics of Geomaterials. *Proc. IS-Seoul*, Pub. Hanrimwon, Seoul, Vol. 1, Eds. Chung et al, 386-395.

API RP2GEO (2011). API Recommended Practice, Geotechnical and Foundation Design Considerations, First Edition, April 2011.

Arroyo, M., Butlanska, J., Gens, A., Calvetti, F., and Jamiolkowski, M. (2011). Cone penetration tests in a virtual calibration chamber. *Géotechnique*, 61(6), 525-531.

Åstedt, B., Weiner, L., and Holm, G. (1992). Increase in bearing capacity with time for friction piles in silt and sand. *Proc. Nordic Geotechnical Meeting*, 411-416.

Baldi, G., Bellotti, R., Ghionna, V., Jamiolkowski, M., and Pasqualini, E. (1986). Interpretations of CPT's and CPTU's, 2nd part: Drained penetration of sands. *4th International conference on field instrumentation and in-situ measurements*, Singapore, 143-156.

Bolton M.D., Gui, M.W., Garnier J., Corte J.F., Bagge, G., Laue, J., and Renzi, R. (1999). Centrifuge cone penetration tests in sand. *Géotechnique*,49(4), 543-552.

Campos, J.L.E., Vargas, E.A., Bernardes, G., Ibañez, J.P., and Velloso, R.Q. (2005). Numerical experiments with discrete elements to simulate pile penetration in granular soils. *Proc. the XXVI Iberian Latin-American Congress on Computational Methods in Engineering* – CILAMCE 2005, Brazilian Assoc. for Comp. Mechanics (ABMEC) & Latin American Assoc. of Comp. Methods in Engineering (AMC), Guarapari, Espírito Santo, Brazil, 19th – 21st October 2005, 8p.

Chow, F.C. (1997). *Investigations into displacement pile behaviour for offshore foundations*. PhD thesis, Imperial College, London, UK.

Chow, F.C., Jardine, R. J., Brucy, F., and Nauroy, J.F. (1998). The effects of time on the capacity of pipe piles in dense marine sand. *Journal of Geotechnical and Geoenvironmental Engineering*, ASCE, 124(3), 254-264.

Clausen, C.J.F., Aas, P.M., and Karlsrud, K. (2005). Bearing capacity of driven piles in sand, the NGI approach. In Gourvenec S and Cassidy M (eds.). *Proc. Int. Symp. on Frontiers in Offshore Geotechnics*: ISFOG 2005. London: Taylor and Francis, 677–683.

de Nicola, A., and Randolph, M.F. (1997). Plugging behaviour of driven and jacked piles in sand. *Géotechnique*, 47(4), 841-856.

Doherty, P., and Gavin, K. (2010). A statistical review of CPT data and the implications for pile design. *2nd International Symposium on Cone Penetration Testing* (CPT10), Paul Mayne eds., Huntington Beach, CA, USA.

Einav, I. (2012). Personal communication.

Feng, T.W., Chen, K.H., Su, Y.T., and Shi, Y.C. (2000). Laboratory investigation of efficiency of conical-based pounders for dynamic compaction. *Géotechnique*, 50(6), 667–674.

Foray, P. (1991). Scale and boundary effects on calibration chamber pile tests. Proc. 1st Int. Conf. on Calibration Chamber Testing, Clarkson University, Postdam, N.Y., 147-161.

Foray, P., Colliat, J-L., and Nauroy, J.F. (1993). Bearing capacity of driven model piles in dense sands from calibration chamber tests. *Proc. 25th Offshore Technology Conference*, Houston, Tex., May 1993, OTC Paper 7194, Vol. 2, 655-665.

Foray, P., Balachowski, L., and Colliat, J-L. (1998). Bearing capacity of model piles driven into dense overconsolidated sands. *Can. Geotech. J.* 35, 374-385.

Gaudin, C., Schnaid, F., and Garnier, J. (2005). Sand characterization by combined centrifuge and laboratory tests. *Int. J. Phys. Modelling Geotech.*, 5(1), 42–56.

Gavin, K.G., and Lehane, B.M. (2003). The Shaft capacity of pipe piles in sand. *Canadian Geotechnical Journal*, 40(1), 36-45.

Golightly, C.R., and Nauroy, J-F.(1990). End bearing capacity of piles in calcareous sands.OTC 1990, *Offshore Technology 22nd annual Conference*, Vol.1, Houston, Texas, USA 7-10 May 1990, OTC-6239, 345-356.

Grabe, J., and Henke, S. (2010). High-performance finite element and coupled Eulerian-Lagrangian simulations of pile installation processes. *Proc. 4th Inter. Conf. Structural Engineering*, Mechanics and Computation in Cape Town (South Africa), CRC Press, 68-73.

Henke, S., and Grabe, J. (2006). Simulation of pile driving by 3-dimensional Finite-Element analysis. *Proc. 17th European Young Geotechnical Engineers' Conference*, Zagreb, Crotia, ed. By V. Szavits-Nossan, Croatian Geotechnical Society, 215-233.

Henke, S., and Grabe, J. (2007). Simulation of pile installation by three-dimensional Finite Element analyses. DarmstadtGeotechnics, 15,179-192.

Henke, S. (2008). *Herstellungseinflüsse aus Pfahlrammung im Kaimauerbau*, PhD Thesis, Veröfentlichungen des Instituts für Geotechnik und Baubetrieb der TU Hamburg-Harburg, vol. 18.

Henke S., Qiu G., and Grabe, J. (2010). A Coupled Eulerian Lagrangian Approach to Solve Geotechnical Problems Involving Large Deformations. *Proc. of 7th European Conference on Numerical Methods in Geotechnical Engineering* (NUMGE) in Trondheim/Norway, 233-238.

Herle, I. (1997). *Hypoplastizität und Granulometrieeinfacher Korngerüste*, PhD thesis. Institut für Bodenmechanik und Felsmechanik der Universität Karlsruhe, Karlsruhe, Vol. 142.

Ho, T.Y.K., Jardine, R.J., and Minh, N.A. (2011). Large displacement interface shear between steel and granular media. *Géotechnique*, 61(3), 221-234.

Huang, A.B., and Hsu, H.H. (2005). Cone penetration tests under simulated field conditions. *Géotechnique* 55(5), 345–354.

Jardine, R.J., Chow, F. C., and Overy, R. (2005). ICP Design methods for driven piles in sands and clays, Thomas Telford, London, UK.

Jardine, R.J., Standing, J.R., and Chow, F.C. (2006). Some observations of the effects of time on the capacity of piles driven in sand. *Géotechnique*, 56(4), 227-244.

Jardine, R.J., and Chow, F.C. (2007). Some developments in the design of offshore Piles. Keynote Paper. *Proc 6th Int. Conf. on Offshore Site Investigations and Geotechnics*, SUT London, 303-332.

Jardine, R.J., Zhu, B.T., Foray, P., and Dalton, J.C.P. (2009). Experimental arrangements for the measurements of soil stresses around a displacement pile. *Soils and Foundations*, 49(5), 661-673.

Jardine, R. J., Zhu, B. T., Foray, P., and Yang, Z.X. (2013a). Measurement of stresses around closed-ended displacement piles in sand. *Géotechnique*, 63(1), 1-17.

Jardine, R. J., Zhu, B. T., Foray, P., and Yang, Z.X. (2013b). Interpretation of stress measurements around closed-ended displacement piles in sand. *Géotechnique*,63(8), 613-627.

Kinloch, H, and O'Sullivan, C. (2007). A micro-mechanical study of the influence of penetrometer geometry on failure mechanisms in granular soils. GeoDenver, 2007, GSP 173 *Advances in Measurement and Modeling of Soil Behavior*, 11p.

Klotz, E.U., and Coop, M.R. (2001). An investigation of the effect of soil state on the capacity of driven piles in sands. *Géotechnique*, 51(9), 733-751.

Knudsen, S., Langford, T., Lacasse, S., and Aas, P.M. (2012). Axial capacity of offshore piles driven in sand using four CPT-based methods. *Proc 7th Int. Conf. on Offshore Site Investigations and Geotechnics*, SUT London, 449-457.

Kolk, H.J., Baaijens, A.E., and Senders, M. (2005). Design criteria for piles in silica sands. In

Gourvenec S and Cassidy M (eds.). *Proc. Int. Symp. on Frontiers in Offshore Geotechnics*: ISFOG 2005. London: Taylor and Francis, 711–716.

Lau, Y., Ooi, G., and Wang, Y. (2010). Three-dimensional DEM simulations on pile installation, *Geomechanics and Geotechnics : From Micro to Macro*, Jiang et al. (eds), CRC Press, 579-583.

Lehane, B. M., Jardine, R. J., Bond, A. J., and Frank, R. (1993). Mechanisms of shaft friction in sand from instrumented pile tests. *J. Geotech. Engng., ASCE*, 119(1), 19-35.

Lehane, B.M., Schneider, J.A., and Xu, X. (2005). CPT based design of driven piles in sand for offshore structures. UWA Report, GEO: 05345

Levacher, D., Morice, Y., Favraud, C., and Thorel, L. (2008). A review of pile drivers for testing in centrifuge, *10th National Coastal Engineering* - Civil Engineering, Instrumentation, measurement, imaging and remote sensing. October 14-16, 2008, Sophia Antipolis, France, 573-583.

Nauroy, J.F., and Le Tirant, P. (1983). Model tests of piles in calcareous sands. *Proceedings of the conference on geotechnical practice in offshore Engineering*, Austin, TX, 356–369.

Overy, R. (2007). The use of ICP design methods for the foundations of nine platforms installed in the UK North Sea. *Proc 6th Int. Conf. on Offshore Site Investigations and Geotechnics*, SUT London, 359-366.

Paik, K., and Salgado, R. (2003). Determination of bearing capacity of open-ended piles in sand. *J. Geotech. Geoenviron. Eng.*, 129(1), 46-57.

Paik, K., Lee, J., and Kim, D. (2011). Axial response and bearing capacity of tapered piles in sandy soil. *Geotechnical Testing Journal*, 34(2), 122-130.

Qiu, G., Henke, S., and Grabe, J. (2011). Application of a coupled Eulerian-Lagrangian approach on geomechanical problems involving large deformations. *Computers and Geotechnics*, 38, 30-39.

Rimoy, S.P. (2013). *Ageing and axial cyclic loading studies of displacement piles in sands*. PhD thesis, Imperial College London.

Sakr, M., and Naggar, M. (2003). Centrifuge modeling of tapered piles in sand. *Geotechnical Testing Journal*, 26(1), 1-13.

Salgado, R., Mitchell, J. K., and Jamiolkowski, M. (1998). Calibration chamber size effects on penetration resistance in sand. *Journal of Geotechnical and Geoenvironmental Engineering*, ASCE, 124(9), 878–888.

Sheng, D., Dieter Eigenbrod, K., and Wriggers, P. (2005). Finite element analysis of pile installation using large-slip frictional contact. *Computers and Geotechnics*, 32(1), 17-26.

White, D.J., and Lehane, B.M. (2004). Friction fatigue on displacement piles in sand. *Géotechnique*, 54(10), 645–658.64.

White, D.J., Schneider, J.A., and Lehane, B.M. (2005). The influence of effective area ratio on shaft friction of displacement piles in sand. In Gourvenec S and Cassidy M (eds.). *Proc. Int. Symp. on Frontiers in Offshore Geotechnics*: ISFOG 2005. London: Taylor and Francis, 741–749.

Yang, Z.X., Jardine, R.J., Zhu, B.T., Foray, P., and Tsuha, C.H.C. (2010). Sand grain crushing and interface shearing during displacement pile installation in sand, *Géotechnique*, 60(6), 469-482.

Zhang, C., Nguyen, G.D., and Einav, I. (2013). The end-bearing capacity of piles penetrating into crushable soils, *Géotechnique*, 63(5), 341-354.

Zhu, B.T., Jardine, R.J., and Foray, P. (2009). The use of miniature soil stress measuring sensors in applications involving stress reversals. *Soils and Foundations*, 49(5), 675-688.

Figure caption list

Fig. 1 Schematic of Mini-ICP1 test showing one example instrument layout; after Jardine et al. (2009)

Fig. 2 Cone resistance q_c profiles for alternative top-membrane designs; after Jardine et al. (2013a) and Zhang et al. (2013)

Fig. 3 Typical CPT profiles: (a) LCPC centrifuge test in Fontainebleau sand from Gaudin et al. (2005); (b) field condition of in uniform dense sand at Blessington test site (Ireland), from Doherty and Gavin (2010)

Fig. 4 Radial stress contours during installation shown at two scales: above (a) 'moving' conditions at the end of each push (σ'_{rm}), and below (b) 'stationary' at the end of each pause (σ'_{rs}), normalized by q_c, shown in %. Dashed curves show locus connecting maxima developed in each case; after Jardine et al. (2013b)

Fig. 5 Comparative 'moving' and 'stationary' radial stresses at (a) r/R=2 and (b) r/R=3 developed during steady penetration against relative pile tip depth h/R

Fig. 6 Profiles interpreted for four h/R values of stationary (a) radial effective stresses and (b) circumferential stresses developed after final stroke of Mini-ICP installation; after Jardine et al (2013b).

Fig. 7 Comparison of soil stresses measured in ICP tests and Gavin and Lehane's CC tests; re-plotted from Gavin and Lehane (2003).

Fig. 8 Comparison of radial stresses measured in ICP tests and Allard's centrifuge tests; from Allard (1990)

Fig. 9 Comparison of radial stresses developed during steady penetration as (a) simulated in analysis by Sheng et al. (2005); (b) measured in Mini-ICP tests

Fig. 10 Comparison between radial stresses (a) numerical predictions made with two h/R values by Qiu et al. (2011); (b) numerical predictions made with three initial densities by Henke et al. (2010).

Fig. 11 Normalized stresses developed at various h/R positions from numerical simulations by Einav (2012): (a) radial and (b) circumferential stresses

Fig. 12 Stress profiles established experimentally and analytically close to pile cone tip during penetration: (a) radial stress; (b) circumferential stress; (c) vertical stress

Notation

D	Diameter, $D_{chamber}$ and D_{pile} are calibration chamber and pile diameters, respectively
D_r	Relative density of sand
d_{50}	Particle diameter that 50% point on particle size distribution
e_0	Initial void ratio
σ'_1, σ'_2, σ'_3	Major, intermediate and minor principal effective stresses
σ'_r	Effective radial stress; σ'_{rm}, σ'_{rs}, σ'_{rmax} are moving, stationary and maximum values
σ'_{rc}	Equalized radial effective stress
σ'_θ	Effective circumferential stress; $\sigma'_{\theta m}$, $\sigma'_{\theta s}$, $\sigma'_{\theta max}$ are moving, stationary and maximum values
σ'_z	Effective vertical stress; σ'_{zm}, σ'_{zs}, σ'_{zmax} are moving, stationary and maximum values; σ'_{z0} is free-field vertical effective stress
q_c	CPT cone resistance
h	Height above pile tip (positive) or depth below pile tip (negative)
L_p	Pile penetration depth
z	Depth below sand surface
R	Pile radius
R^*	Equivalent radius of an open-ended pile
R_0	Outer radius of an open-ended pile
R_i	Inner radius of an open-ended pile
r	Radius of point from pile axis
τ_{rzf}	Local shaft resistance of piles

K_A	Rankine coefficients of active earth pressure
φ'	Effective angle of shearing resistance, φ'_{cs} is critical state value
δ'	Effective angle of interface shearing resistance
p_A	The atmospheric pressure
z	Depth below the sand surface
z_{tip}	Depth of pile tip below the sand surface

Figure Caption List

Fig. 1 Schematic of Mini-ICP1 test showing one example instrument layout; after Jardine et al. (2009)

Fig. 2 Cone resistance q_c profiles for alternative top-membrane designs; after Jardine et al. (2013a) and Zhang et al. (2013)

Fig. 3 Typical CPT profiles: (a) LCPC centrifuge test in Fontainebleau sand from Gaudin et al. (2005); (b) field condition of in uniform dense sand at Blessington test site (Ireland), from Doherty and Gavin (2010)

Fig. 4 Radial stress contours during installation shown at two scales: above (a) ‘moving’ conditions at the end of each push (σ'_{rm}), and below (b) ‘stationary’ at the end of each pause (σ'_{rs}), normalized by q_c, shown in %. Dashed curves show locus connecting maxima developed in each case; after Jardine et al. (2013b)

Fig. 5 Comparative 'moving' and 'stationary' radial stresses at (a) r/R=2 and (b) r/R=3 developed during steady penetration against relative pile tip depth h/R

Fig. 6 Profiles interpreted for four h/R values of stationary (a) radial effective stresses and (b) circumferential stresses developed after final stroke of Mini-ICP installation; after Jardine et al (2013b)

Fig. 7 Comparison of soil stresses measured in ICP tests and Gavin and Lehane’s CC tests; replotted from Gavin and Lehane (2003)

Fig. 8 Comparison of radial stresses measured in ICP tests and Allard’s centrifuge tests; from Allard (1990)

Fig. 9 Comparison of radial stresses developed during steady penetration as (a) simulated in analysis by Sheng et al. (2005); (b) measured in Mini-ICP tests

Fig. 10 Comparison between radial stresses (a) numerical predictions made with two h/R values by Qiu et al. (2011); (b) numerical predictions made with three initial densities by Henke et al. (2010)

Fig. 11 Normalized stresses developed at various h/R positions from numerical simulations by Einav (2012): (a) radial and (b) circumferential stresses

Fig. 12 Stress profiles established experimentally and analytically close to pile cone tip during penetration: (a) radial stress; (b) circumferential stress; (c) vertical stress

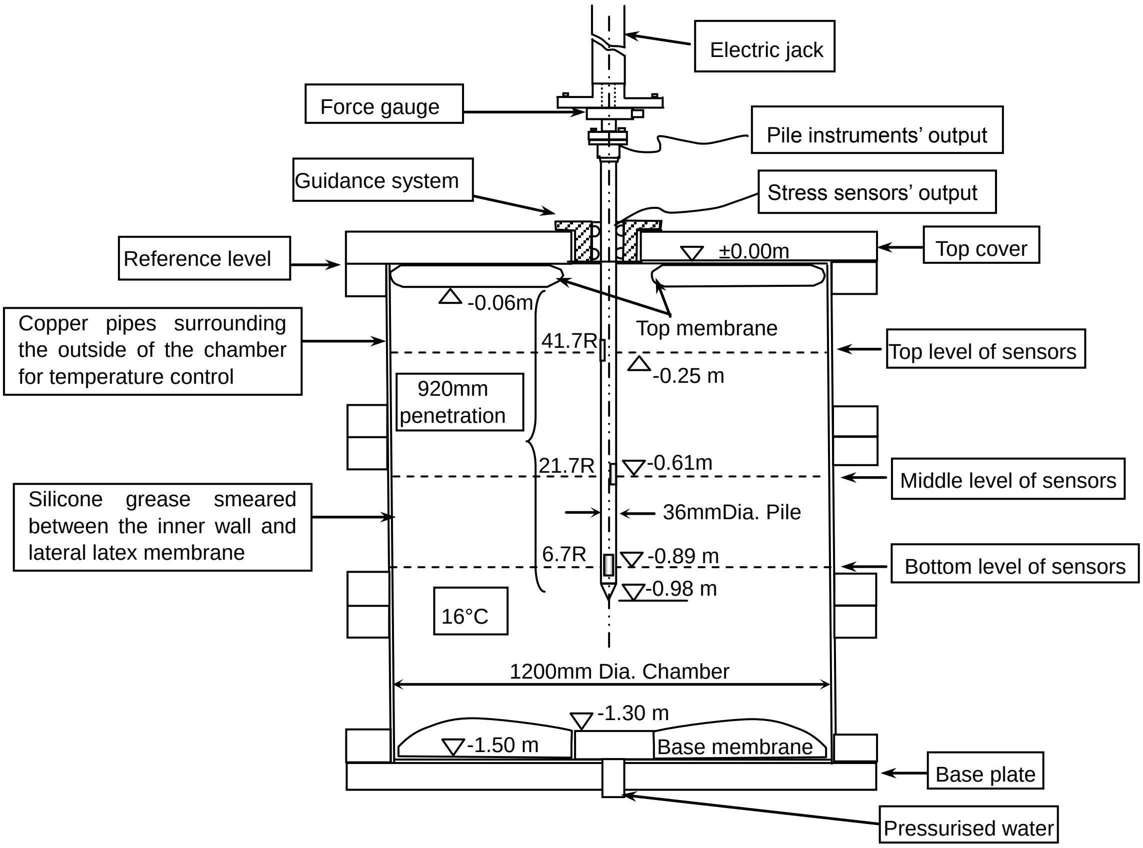

Fig. 1 Schematic of Mini-ICP1 test showing one example instrument layout; after Jardine et al. (2009)

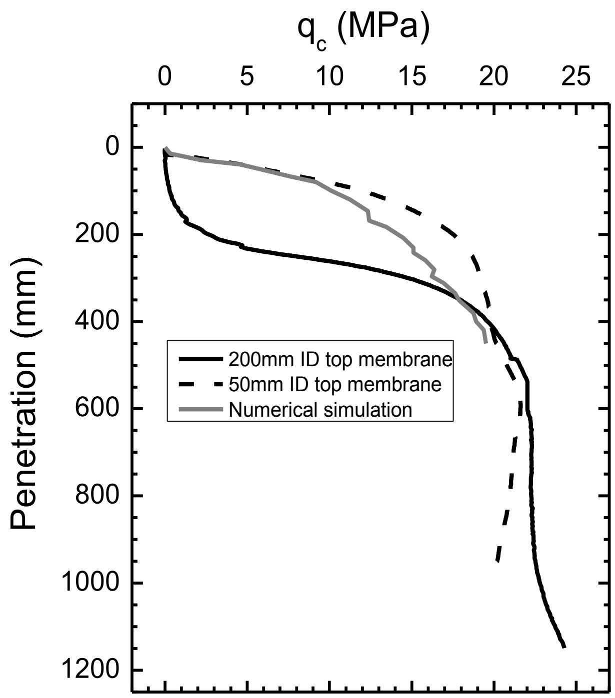

Fig. 2 Cone resistance q_c profiles for alternative top-membrane designs; after Jardine et al. (2013a) and Zhang et al. (2013)

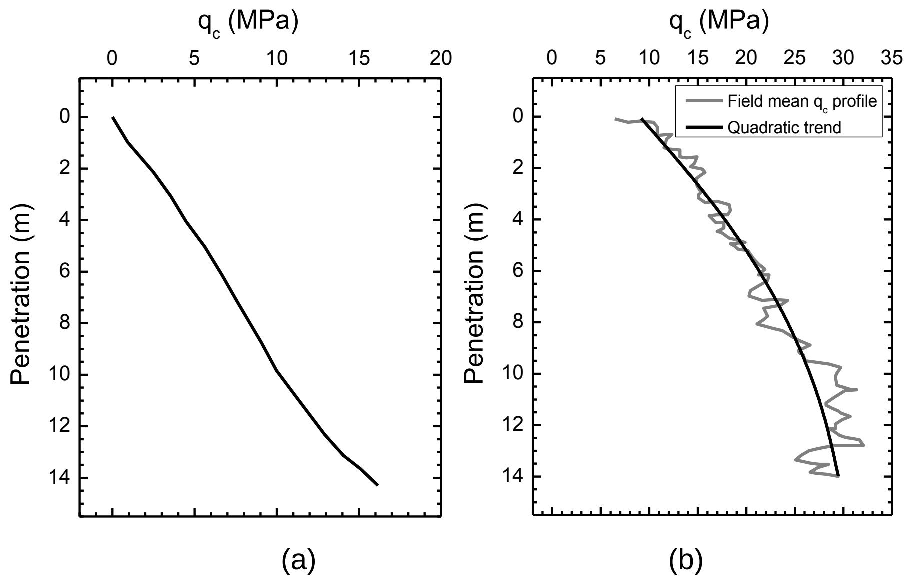

Fig. 3 Typical CPT profiles: (a) LCPC centrifuge test in Fontainebleau sand from Gaudin et al. (2005); (b) field condition of in uniform dense sand at Blessington test site (Ireland), from Doherty and Gavin (2010)

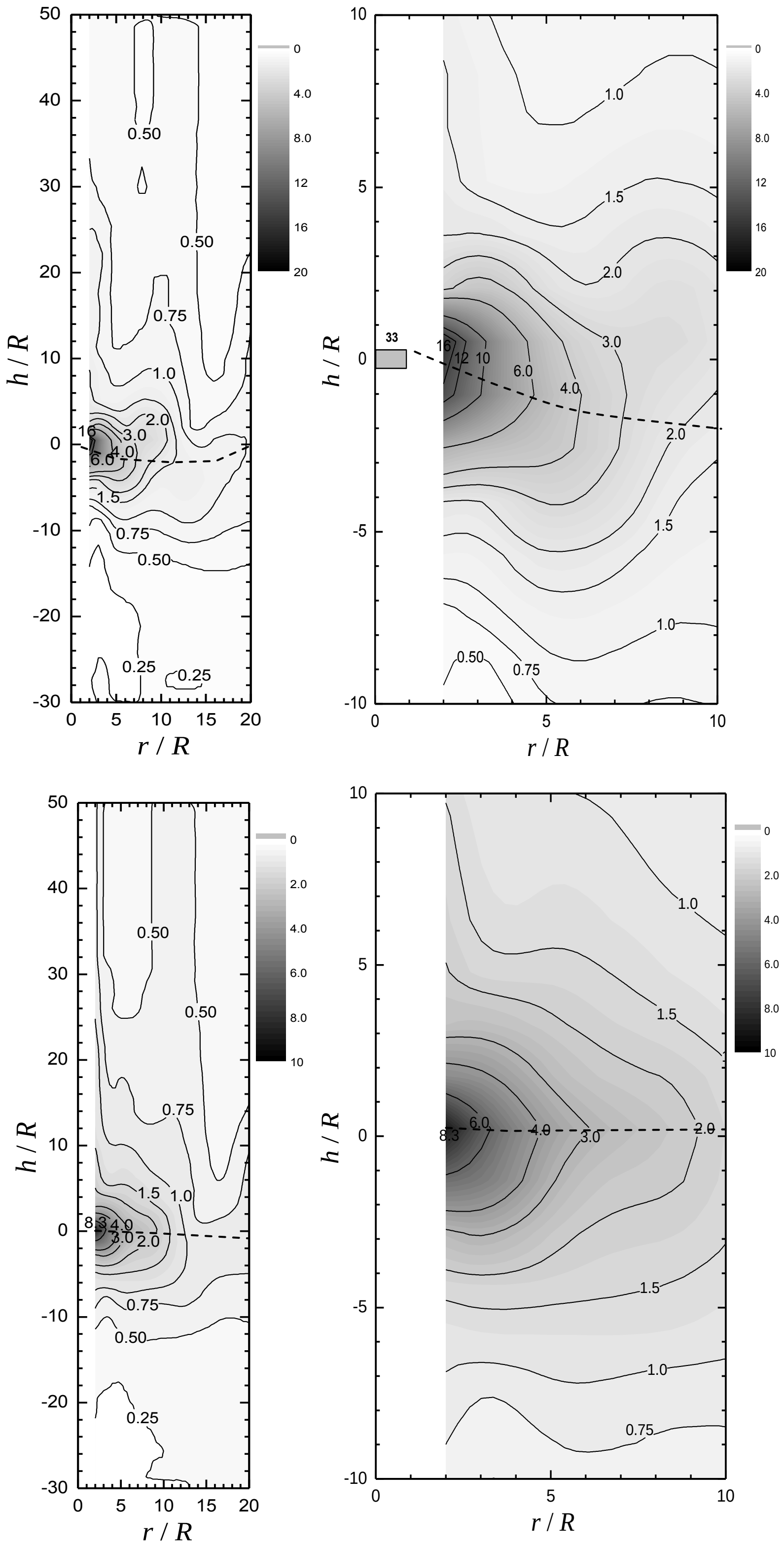

Fig. 4 Radial stress contours during installation shown at two scales: above (a) 'moving' conditions at the end of each push (σ'_{rm}), and below (b) 'stationary' at the end of each pause (σ'_{rs}), normalized by q_c, shown in %. Dashed curves show locus connecting maxima developed in each case; after Jardine et al. (2013b)

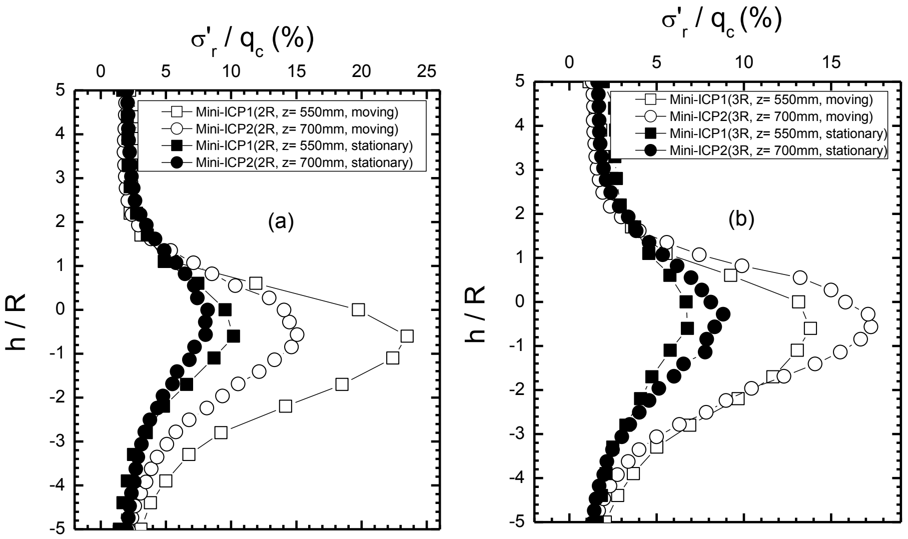

Fig. 5 Comparative 'moving' and 'stationary' radial stresses at (a) r/R=2 and (b) r/R=3 developed during steady penetration against relative pile tip depth h/R

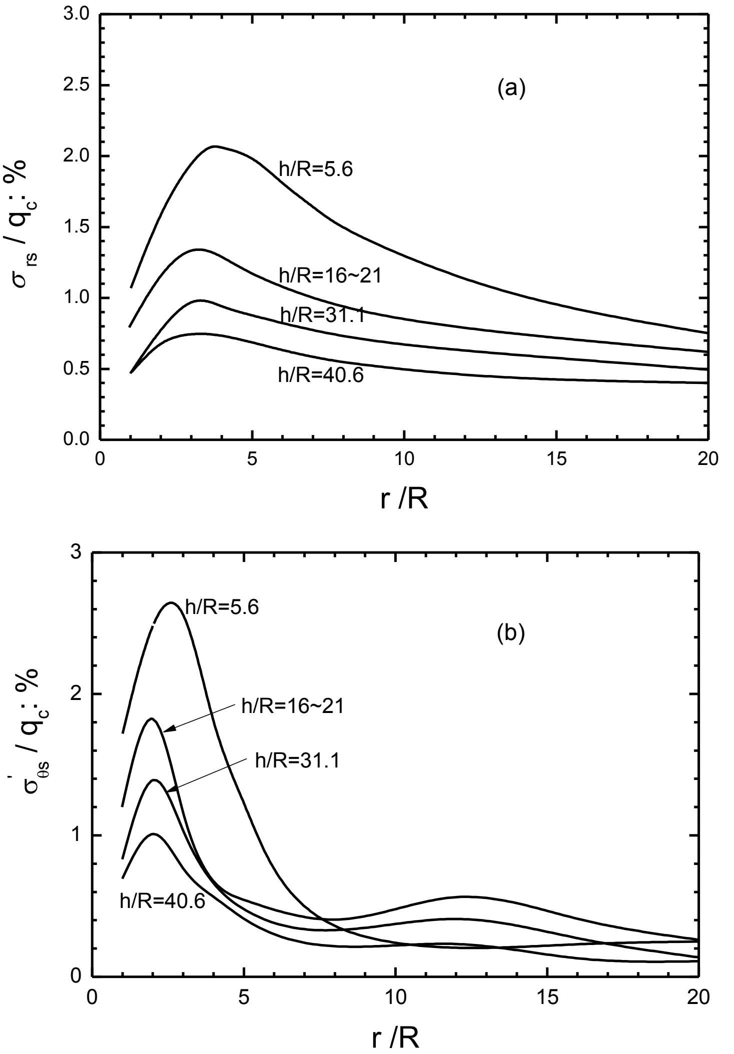

Fig. 6 Profiles interpreted for four h/R values of stationary (a) radial effective stresses and (b) circumferential stresses developed after final stroke of Mini-ICP installation; after Jardine et al (2013b).

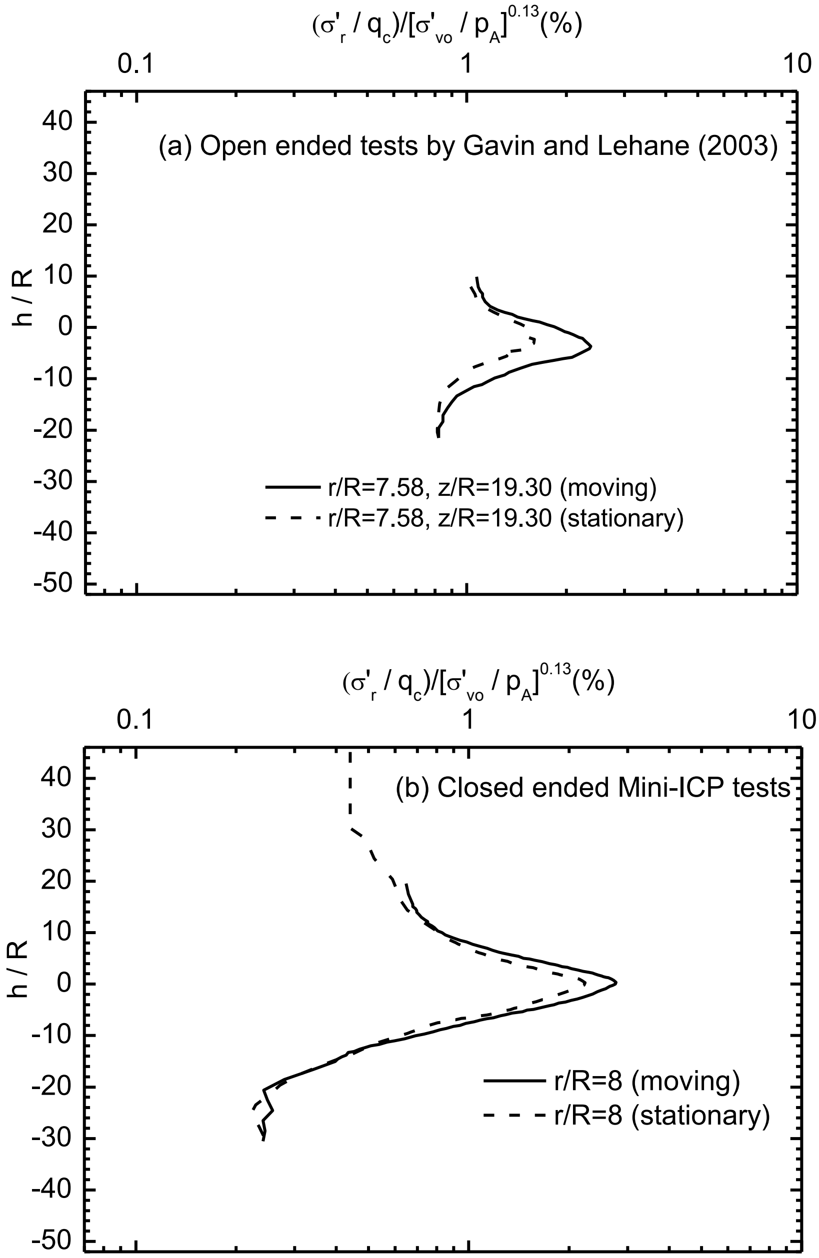
(σ'r / qc)/[σ'vo / pA]^0.13(%)
0.1
1
10
(a) Open ended tests by Gavin and Lehane (2003)
h / R
40
30
20
10
0
-10
-20
-30
-40
-50
r/R=7.58, z/R=19.30 (moving)
r/R=7.58, z/R=19.30 (stationary)
(σ'r / qc)/[σ'vo / pA]^0.13(%)
0.1
1
10
(b) Closed ended Mini-ICP tests
h / R
40
30
20
10
0
-10
-20
-30
-40
-50
r/R=8 (moving)
r/R=8 (stationary)

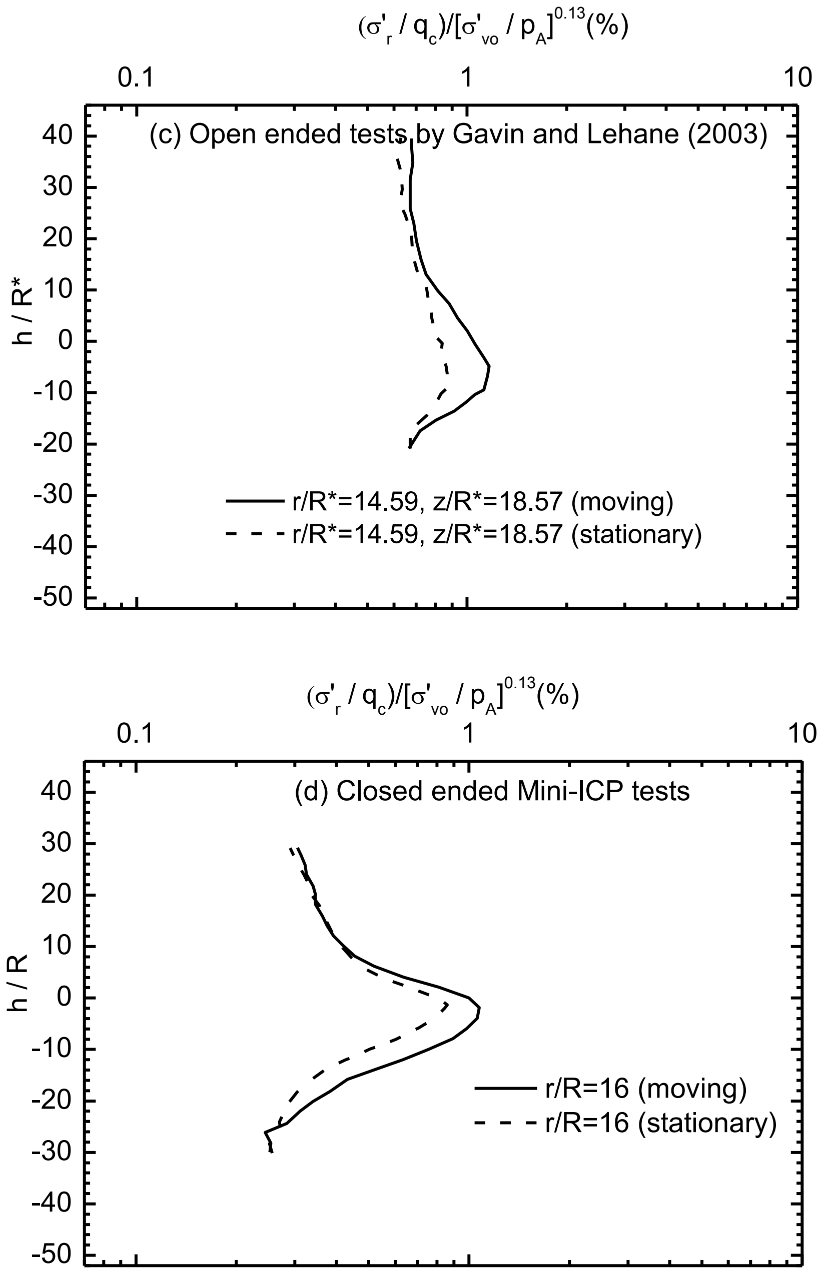

Fig. 7 Comparison of soil stresses measured in ICP tests and Gavin and Lehane's CC tests; replotted from Gavin and Lehane (2003).

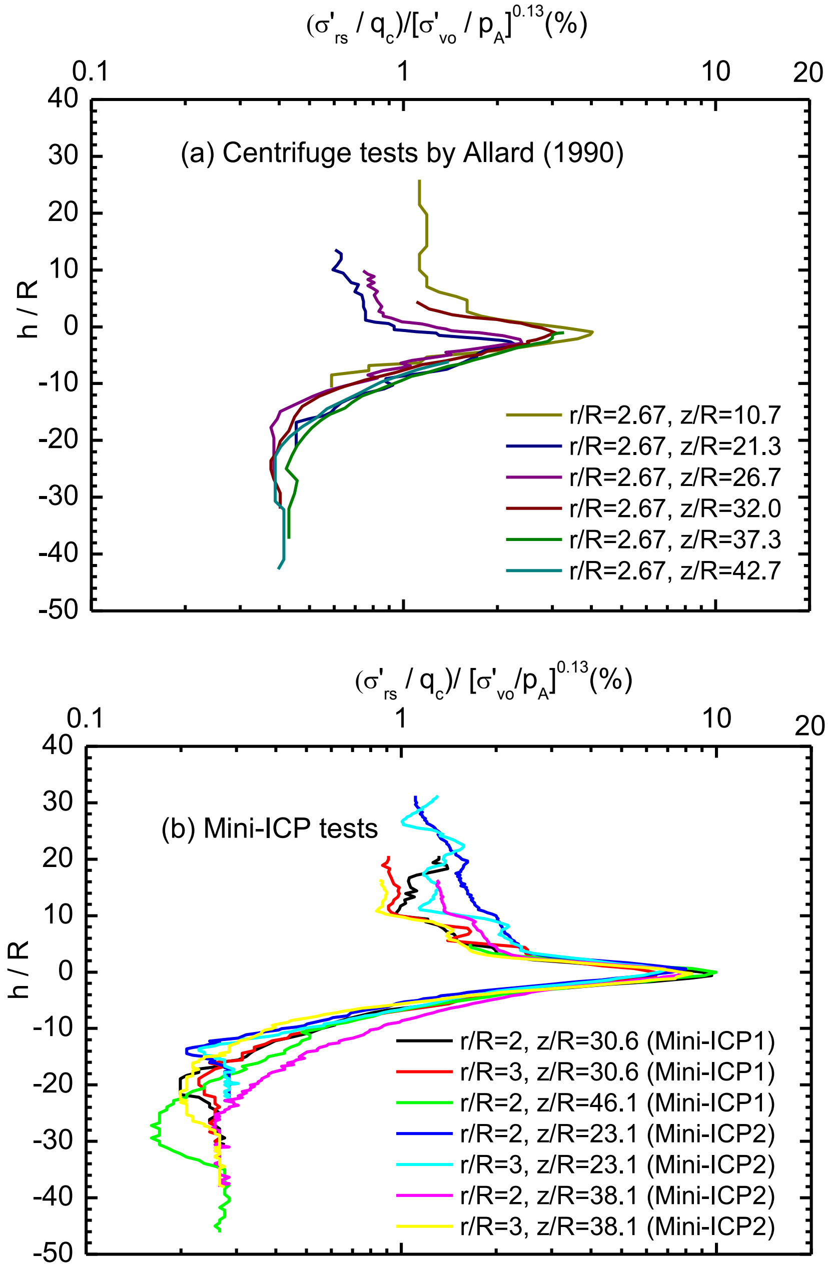

Fig. 8 Comparison of radial stresses measured in ICP tests and Allard's centrifuge tests; from Allard (1990)

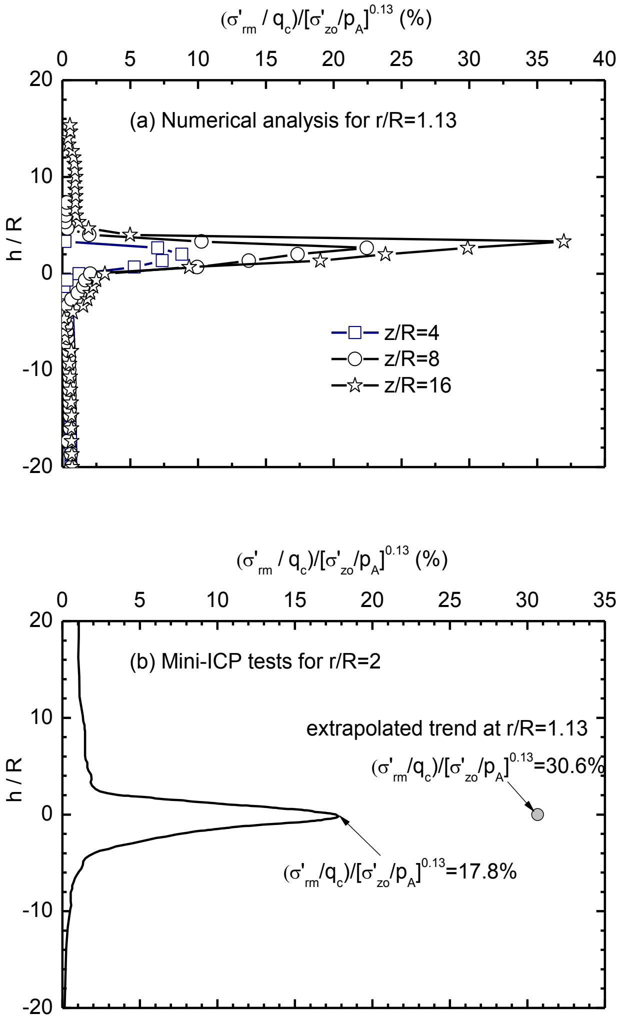

Fig. 9 Comparison of radial stresses developed during steady penetration as (a) simulated in analysis by Sheng et al. (2005); (b) measured in Mini-ICP tests

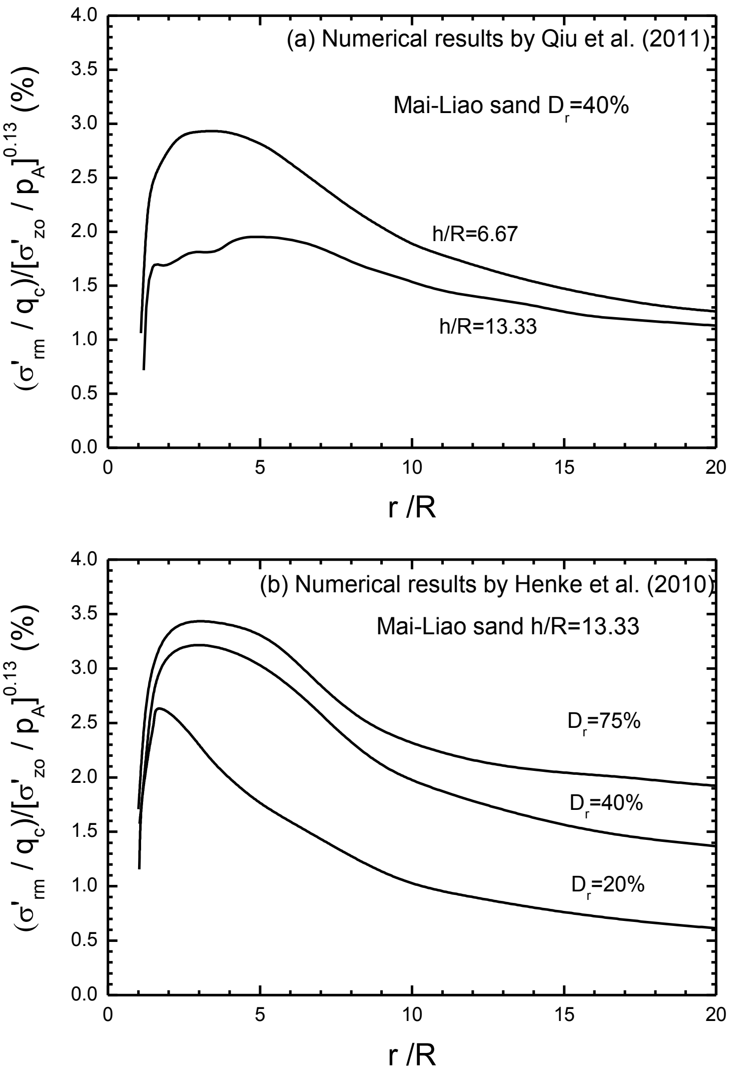

Fig. 10 Comparison between radial stresses (a) numerical predictions made with two h/R values by Qiu et al. (2011); (b) numerical predictions made with three initial densities by Henke et al. (2010).

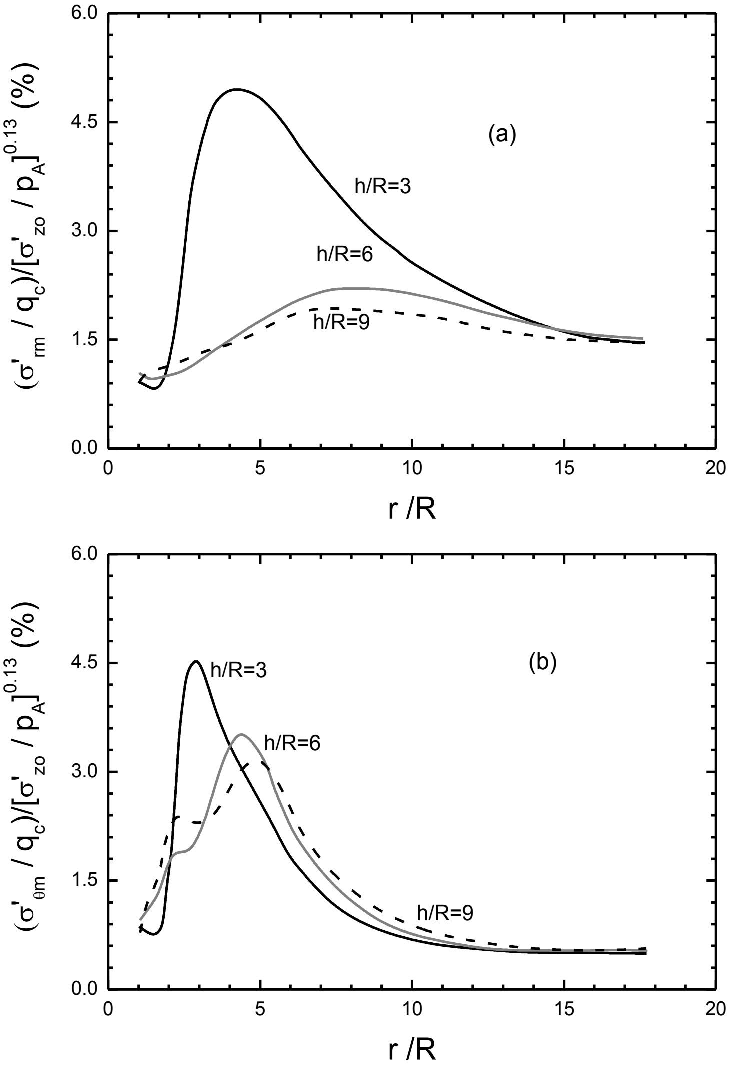

Fig. 11 Normalized stresses developed at various h/R positions from numerical simulations by Einav (2012): (a) radial and (b) circumferential stresses

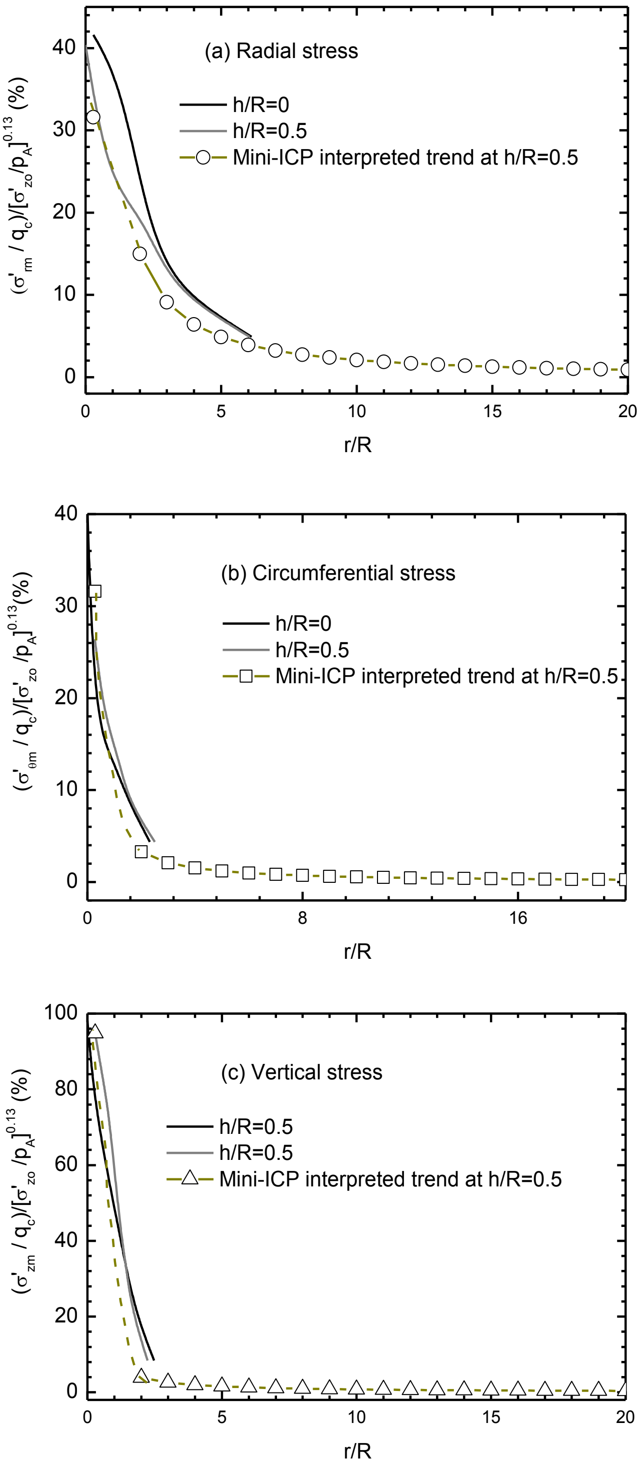

Fig. 12 Stress profiles established experimentally and analytically close to pile cone tip during penetration: (a) radial stress; (b) circumferential stress; (c) vertical stress

Table 1 Summary of key features of considered stress measurements or predictions (N/A=not available; NA=not applicable; CC=calibration chamber)

Reference	Method	Chamber Internal Diameter (mm)	Sand		D_{pile}/d_{50}	$D_{chamber}/D_{pile}$	Boundary conditions			Sensor calibration	Pile and installation method			
			d_{50} (mm)	Dr (%)			Surcharge/ acceleration (kPa)	Lateral boundary	Chamber wall Friction		Type	D_{pile} (mm)	L_p (mm)	Installation No. of cycles (N)
Jardine et al (2009, 2013a, b)	CC test	1,200	0.21	72	171	33.3	150~200	Rigid	Minimised by latex membrane	Non-linear loading-unloading	Closed-ended Cone	36	920-1000	Jacking cycles N=50~200
Allard (1990)	Centrifuge	152	0.1	57.5	95	16.0	50g	Rigid	N/A	Non-linear loading-unloading	Closed-ended Flat	9.5	188	Driving N_{blow}=240~300
Gavin & Lehane (2003)	CC test	1,680	0.22	30±2	518	14.7	40kPa bottom	Rigid	Reduced by smooth HDPE lining	N/A	Open-ended Flat	114	1600	Jacking cycles N=16
Sheng et al. (2005)	FEM	580	0.32	76	94	19.3	66.7g	Rigid	0	NA	Closed-ended Cone	30	230	Steady pushing N=1
Henke et al. (2010) & Qiu et al. (2011)	FEM	10,000	0.16*	20,40 and 75	1875	33.3	1g	Rigid	0	NA	Closed-ended Cone	300	5000	Steady pushing N=1
Zhang et al. (2013) & Einav (2012)	FEM	The axis-symmetric FE model simulating CC tests reported by Jardine et al (2013a, b)								N/A	Closed-ended Cone	36	450	Steady pushing N=1

* The d_{50}=0.16mm of Mai-Liao sand is sourced from Feng et al. (2000) while not specified in Henke et al (2010) or Qiu et al (2011).